Nanoscale

Accepted Manuscript

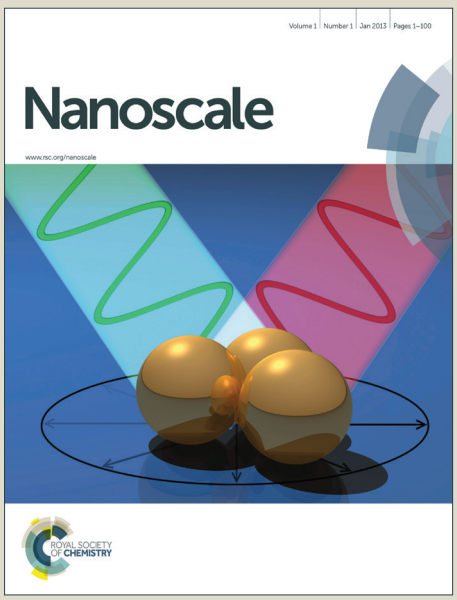

ROYAL SOCIETY OF CHEMISTRY

www.rsc.org/nanoscale

ARTICLE TYPE www. rsc.org/xxxxxx | XXXXXXXX

Elastic limit of silicane

Qing Peng * **and Suvranu De**

Silicane is a fully hydrogenated silicene–a counterpart of graphene–having promising applications in hydrogen storage with capacities larger than 6 wt%. Knowledge of its elastic limit is critical in its applications as well as tailoring its electronic properties by strain. Here we investigate the mechanical response of silicane to various strains using first-principles calculations based on density functional theory. We illustrate that non-linear elastic behavior is prominent in the two-dimensional nanomaterials as opposed to bulk materials. The elastic limits defined by ultimate tensile strains are 0.22, 0.28, and 0.25 along armchair, zigzag, and biaxial directions, respectively, an increase of 29%, 33%, and 24% respectively in reference to silicene. The in-plane stiffness and Poisson ratio are reduced by a factor of 16% and 26%, respectively. However, hydrogenation/dehydrogenation has little effect on its ultimate tensile strengths. We obtained high order elastic constants for a rigorous continuum description of the nonlinear elastic response. The limitation of second, third, fourth, and fifth order elastics are in strain range of 0.02, 0.08, and 0.13, and 0.21, respectively. The pressure effect on the second order elastic constants and Poisson's ratio were predicted from the third order elastic constants. Our results could provide a safe guide for promising applications and strain-engineering the functions and properties of silicane monolayers.

1 INTRODUCTION

As the silicon-based counterpart of graphene, silicene gives rise to intense interest due to the promise of an easily implemented way to improve the performance and scalability of electronic silicon devices without departure from the silicon-based status quo, which is a crucial advantage and a large cost reduction [1–9]. The fully saturated hydrogenation of silicene, so-called "silicane" (Fig. 1), is a subject of interest in the field of modern silicon based nanotechnology in addition to the field of hydrogen storage. For example, high hydrogen capacities of Li-decorated (6.3 wt% [10,11]) and K-decorated (6.13 wt% [12]) silicane have been reported very recently, in excess of 6 wt%, the U. S. Department of Energy target.

Despite studies on the structural, electronic, magnetic, and optical properties of silicane [12–24], as well as its applications [10,12], there are questions which are still not answered: What is the elastic limit of silicane? What are nonlinear elastic properties? The answers to these questions are critical in designing parts or structures with this advanced material, as well as in regarding their practical applications. Knowledge of the elastic limit can be served as a guide, for example, in strain engineering, which is a common and important approach to tailor the functions and properties of nanomaterials [17,23,25–27]. The non-linear elastic properties are indispensable because these 2D materials are vulnerable to strain with or without intent due to their monatomic thickness. For instance, there are strains caused by the mismatch of lattices or surface corrugation due to the presence of a substrate.

It is generally accepted that the armchair-like structure of silicane is the most energetically favorable and thus the most

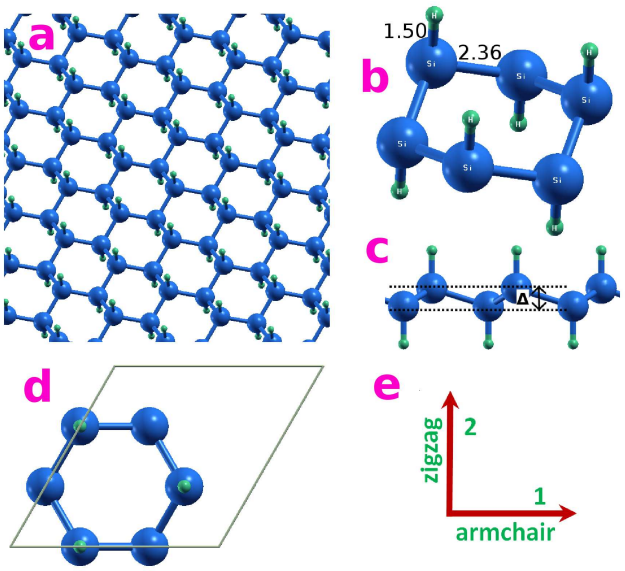

Fig. 1 Configurations of silicane. a Silicane plane. **b** Hexagonal rings tilt and **c**side views. **d** Conventional unit cell and simulation box. **e** Orientations and directions of simulation cells.

Address: Department of Mechanical, Aerospace and Nuclear Engineering, Rensselaer Polytechnic Institute, Troy, NY 12180, U.S.A.
* *Email: qpeng.org@gmail.com,Tel: 518-279-6669;*

stable configuration[14,21]. Opposite to the zero band gap of silicene, silicane has a large band gap of 4.0 eV[13,15,16,21] which is indirect at zero strain, transforming to direct under a linear strain of 0.05[26], then disappearing beyond a strain of 0.2[17,26]. The in-plane stiffness and Poisson ratio are predicted as 52.55 N/m and 0.24, respectively[17], as well as their chirality dependence[26]. The tunable gaps and enhanced mobilities in strain-engineered silicane are also reported[27]. However, the higher order elastic constants of silicane, which describe the nonlinear behaviors, have not been studied. Higher order elastic constants are important quantities[28] and can be determined by measuring the changes of sound velocities under the application of hydrostatic and uniaxial stresses[29]. The higher order elastic constants can be utilized to study the nonlinear elasticity, thermal expansion (through the gruneisen parameter), temperature dependence of elastic constants, harmonic generation, phonon-phonon interactions, photon-phonon interactions, lattice defects, phase transitions, echo phenomena, strain softening, and so on[30].

The goal of this paper is to study the elastic limit and nonlinear mechanical properties of silicane, and find an accurate continuum description of the elastic properties from *ab initio* density functional theory calculations. The mechanical response and the elastic limits including ultimate strengths and ultimate strains were studied under varies strains. The high order elastic constants up to fifth order were obtained by fitting the stress-strain curves to analytical stress-strain relationships. Moreover, the pressure effect on the second order elastic constants, in-plane stiffness, and Poisson ratio, are predicted. Our continuum formulation results are useful in finite element modeling of the mechanical properties of silicane at the continuum level because our results of ideal strengths provide an upper limit of the strength at macroscopic scale which might contain defects. In addition, modeling defect-free systems at the continuum level is also a practical and interesting topic since such kinds of defect-free materials were reported in large scale in the nanoindentation experiments[31].

2 COMPUTATIONAL METHOD

We consider a conventional cell ($\sqrt{3}\times\sqrt{3}$ cell) which contains 12 atoms (6 silicon atoms and 6 hydrogen atoms) for silicane (Fig. 1) with periodic boundary conditions. Such a conventional unit cell is chosen to capture the "soft mode", which is a particular normal mode exhibiting an anomalous reduction in its characteristic frequency and leading to mechanical instability[32]. This soft mode is a key factor in limiting the strength of monolayer materials that can only be captured in unit cells with hexagonal rings[32].

The total energies of the system, forces on each atom, stresses, and stress-strain relationships under the desired deformation configurations are characterized via first-principles calculations based on density-functional theory (DFT). DFT calculations were carried out with the Vienna Ab-initio Simulation Package (VASP)[33] which is based on the Kohn-Sham Density Functional Theory with the generalized gradient approximations as parameterized by Perdew, Burke and Ernzerhof (PBE) for exchange-correlation functions[34]. The electrons explicitly included in the calculations are the ($3s^2 3p^2$) electrons. The core electrons ($1s^2 2s^2 2p^6$) are replaced by the projector augmented wave (PAW) and pseudo-potential approach[35]. A plane-wave basis set with kinetic-energy cutoff of 600 eV is used in all the calculations. The calculations are performed at zero temperature. The criterion to stop the relaxation of the electronic degrees of freedom is set by requiring the total energy change to be smaller than 10^{-6} eV. The optimized atomic geometry was achieved through minimizing Hellmann-Feynman forces acting on each atom until the maximum forces on the ions were smaller than 0.001 eV/Å. The atomic structures of all the deformed and undeformed configurations are obtained by fully relaxing atoms in the unit-cells.

The irreducible Brillouin Zone was sampled with a Gamma-centered $15\times15\times1$ k-mesh. Such a large k-mesh was used to reduce the numerical errors caused by the strain of the systems. The initial charge densities were taken as a superposition of atomic charge densities. There was a 20 Å thick vacuum region to reduce the inter-layer interaction to model the single layer system. To eliminate the artificial effect of the out-of-plane thickness of the simulation box on the stress, we used the second Piola-Kirchhoff (P-K) stress[36] to express the 2D forces per length with units of N/m. The Lagrangian strain is used in this study, defined as $\eta=\varepsilon+1/2\varepsilon^2$, where ε is the stretch ratio[36]. When the strains are applied, all the atoms are allowed full freedom of motion. A quasi-Newton algorithm is used to relax all atoms into equilibrium positions within the deformed unit cell that yields the minimum total energy for the imposed strain state of the super cell.

For a general deformation state, the number of independent components of the second, third, fourth, and fifth order elastic tensors is 21, 56, 126, and 252, respectively. However, only fourteen independent elastic constants need to be explicitly considered due to the symmetries of the atomic lattice point group D_{6h}, which consists of a six-fold rotational axis and six mirror planes[37]. The fourteen independent elastic constants of silicane are determined by a least-squares fit to the stress-strain results from DFT calculations in two steps, detailed in our previous work[36], which have been well used to explore the mechanical properties of 2D materials[38–43]. A brief introduction is that, in the first step, we use a least-squares fit of five stress-strain responses. Five relationships between stress and strain are necessary because there are five independent fifth-order elastic constants (FFOEC). We obtain the stress-strain relationships by simulating the following deformation states: uniaxial strain in the zigzag direction (*zigzag*); uniax-

ial strain in the armchair direction (*armchair*); and equibiaxial strain (*biaxial*). From the first step, the components of the second-order elastic constants (SOEC), the third-order elastic constants (TOEC), and the fourth-order elastic constants (FOEC) are over-determined (i.e, the number of linearly independent variables are greater than the number of constrains), and the fifth-order elastic constants are well-determined (the number of linearly independent variables are equal to the number of constrains). Under such circumstances, the second step is needed: least-square solution to these over- and well- determined linear equations.

3 RESULTS AND ANALYSIS

3.1 Atomic structure

We first optimized our system to determine the equilibrium lattice constants for silicane. The total energy as a function of lattice spacing is obtained by specifying seven lattice constants varying from 3.6 Åto 4.2 Å, with full relaxations of all the atoms. A least-square fit of the energies versus lattice constants with a fourth-order polynomial function yields the equilibrium lattice constant as a=3.89 Å, with Si-Si bond lengths of 2.36 Å, a little bit larger than twice the covalent bond length of silicon of 1.11 Å [48]. This most energetically favorable structure is set as the strain-free structure.

Our result of the structure of the conventional cell of the chair-like configuration of silicane is shown in Fig. 1. For a comparison of the buckling behaviors among different atomic monolayer structures, we define a dimensionless parameter buckling roughness $\rho_b = \Delta/a$ as the ratio of the bucking height Δ to its spacial frequency (lattice constant a here). The geometry parameters including the lattice constant a, characteristic bond length Si-Si and Si-H, sheet buckling height Δ, bond angle Si-Si-Si β and Si-Si-H γ, buckling roughness ρ_b of Silicane, as well as those of silicene and the counterparts of graphane are summarized in Table 1, agreeing well with previous theoretical and experimental results.

In reference to silicene which is low buckled [5,49], the Si-Si bonds in silicane are stretched by a factor of 3.5% while the lattice constant a only increases 0.5%. This indicates that the hydrogenation of silicene has little effect on its in-plane structure. It is not surprising that the silicane structure is similar to the silicene since the silicon atoms have the same type of (sp^3) bonds. The Si-H bonds are perpendicular to the silicon planes (Fig. 1 c) with an effort pulling the silicon atoms out of plane. As a result the buckling height Δ increases greatly by 60%. Compared to graphane, the bond length of Si-Si is 2.36 Å, 1.53 times of that of C-C bond. Interestingly, the differences of bond angles are less than 0.4% despite the large difference in bond lengths and buckling heights. This is a combined effect of their sp^3 bond type and the hydrogenation. Furthermore, by introducing the dimensionless parameter buckling roughness ρ_b, the silicane atomic structures have the high similarities characterized by ρ_b (Table 1).

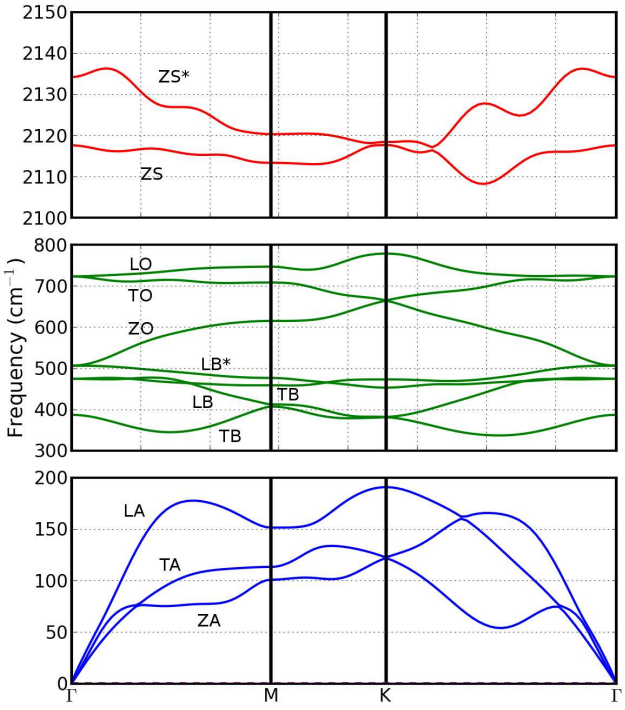

Fig. 2 Phonon dispersion curve The calculated phonon dispersion curves of silicane monolayers at zero temperature and strain-free state.

3.2 Phonon dispersion curve

The dynamical instabilities of a crystal is in general observed through phonon dispersion curves. Our phonon dispersion curves are obtained from density functional perturbation theory calculations implemented in Quantum Espresso [50]. The PAW-PBE pseudo-potentials with kinetic-energy cutoff of 60 Ry (816 eV) for wave-functions is used in this phonon calculations. The kinetic energy cutoff for charge density is 240 Ry (3264 eV). The k-point grid and q-points grid are $24 \times 24 \times 1$ and $8 \times 8 \times 1$, respectively. The calculated phonon dispersion curves of silicane monolayers at zero temperature are displayed in Fig. 2.

There is no soft modes, or negative frequencies, in the phonon dispersion curves along any high-symmetry direction of the Brillouin zone, which indicates that silicane monolayers are dynamically stable at the ground state. The three acoustic phonon bands (blue lines) reflect the long-wave phase motions. They are longitudinal acoustic (LA), transverse acoustic (TA), and flexural acoustic (ZA) modes in the bottom panel

Table 1 Geometry parameters The lattice constant a, characteristic bond length Si-Si and Si-H, sheet buckling height Δ, bond angle Si-Si-Si β and Si-Si-H γ, buckling roughness ρ_b of Silicane from our DFT calculations, compared with previous DFT calculations and experimental results, as well as those of silicene and the counterparts of graphane. All lengths are in Å and angles in degrees.

	Silicane	Calculations[a]	Experiments	Silicene[d]	Graphane[e]
a	3.89	2.82-3.97	3.8-4.1[b]	3.87	2.54
$Si-Si$	2.36	2.32-2.39	2.35[c]	2.28	1.54[f]
$Si-H$	1.50	1.50-1.52	1.15[c]		1.11[g]
Δ	0.72	0.69-0.72		0.45	0.46
β	111.1	110.5-111.6		116.1	111.5
γ	107.7				107.3
ρ_b	0.185	0.18-0.24		0.116	0.181

[a] Ref.[12–22,24]; [b] Ref.[44,45]; [c] Ref.[46]; [d] Ref.[5]; [e] Ref.[47]; [f] $C-C$; [g] $C-H$;

of Fig. 2. These three bands show a linear dependence on the wave vectors around the zone center (Γ points). There are three optical phonon modes which are similar curves with higher frequencies referring to silicene[51] are longitudinal optical (LO), transverse optical (TO), and flexural optical (ZO) modes in the middle panel of Fig. 2. There are two stretching phonon modes along the out-of-plane direction: one is symmetric (ZS) and the other is anti-symmetric (ZS*), shown in the top panel. The rest four phonon modes are related to the bending, divided into two groups (symmetrical and anti-symmetrical) for two directions (longitudinal and transverse), as symmetrical longitudinal bending (LB), symmetrical transverse bending (TB), anti-symmetrical longitudinal bending (LB*), and anti-symmetrical transverse bending (TB*). Our results agrees with previous prediction well[52].

3.3 Strain Energy

We applied the strains in three deformation modes, namely *armchair* for uniaxial strain along the armchair direction, *zigzag* for uniaxial strain along the zigzag direction, and *biaxial* for biaxial strains in both directions. We studied both compressive (negative) and tensile (positive) strains in range of -0.1 to 0.4 with an increment of 0.01 in each step. Such an asymmetrical strain range is selected according to the asymmetrical mechanical responses to the tensile and compressive strains, as demonstrated in the next subsection. It is worth noting that in general the compressive strains will cause rippling of the *free-standing* thin films, membranes, plates, and nanosheets[53]. Take graphene as an example. The critical compressive strain for rippling instability is much less than the critical tensile strain for fracture, for example, 0.0001% versus 2% in graphene sheets[54]. However, the rippling can be suppressed by applying constraints, such as embedding (0.7%)[55], substrate (0.4% before heating)[56], thermal cycling on SiO_2 substrate (0.05%)[57] and BN substrate (0.6%)[58], and sandwiching[59]. Our study of compressive strains is important

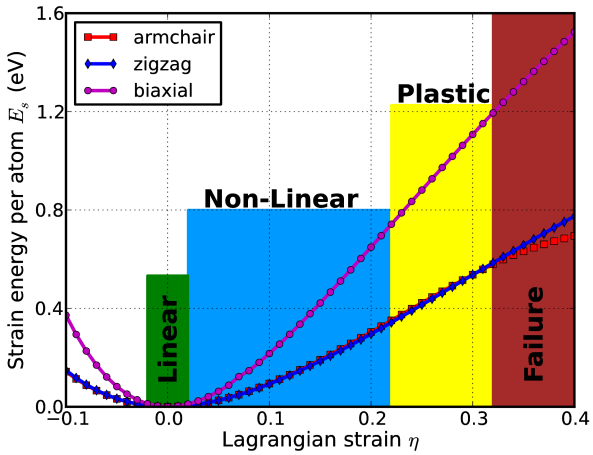

Fig. 3 Energy-strain responses. The strain energy per Si-H pair as a function of Lagrangian strain[36] η under uniaxial deformations along armchair (*armchair*) and zigzag (*zigzag*) directions, and biaxial deformation along both directions (*biaxial*) for both compression ($\eta < 0$) and tension ($\eta > 0$) in a silicane monolayer.

in understanding the mechanics of these non-rippling applications.

Here we define the strain energy per silicon atom as $E_s = (E_{tot} - E_0)/n$, where E_{tot} is the total energy of the strained system, E_0 is the total energy of the strain-free system, and $n = 6$ is the number of silicon atoms in the unit cell. Overall, E_s is non-symmetrical for compression ($\eta < 0$) and tension ($\eta > 0$) for all three modes. This non-symmetry indicates the anharmonicity of the silicane structures. It is also shown that E_s is isotropic in uniaxial tensile strains up to 0.3. In addition, the E_s describes the potential energy profile as a well with a large depth , indicating a wide stable region for the silicane monolayer under various strains.

The strain energy variation with respect to strain (Fig. 3) displays linear elastic, non-linear elastic, plastic, and failure regions. In the linear elastic region, the E_s is a quadratic function of applied strain. The stresses are derivatives of the strain energies with strains. As a result, the stresses are proportional to strains in this region. This linear elastic region is small, $-0.02 < \eta < 0.02$, compared to ultimate strains of silicane monolayers discussed later. In the non-linear elastic region, the linear stress-strain relationship is invalid and higher order terms are not negligible. The E_s is a higher order (anharmonic) function of applied strains. Such region is still considered elastic because when the applied strains are removed, the system will return to the reference equilibrium state of E_0 since there are no defects in the system. However, with larger loading of strains, the systems will undergo irreversible structural changes, and then fail. The maximum strain in the non-linear elastic region is defined as *critical* strain. Under armchair deformation of a silicane monolayer, the critical strain is 0.33 (Fig. 3), larger than that of silicene (0.30). The critical strains were not spotted in the testing range for both materials under zigzag and biaxial deformations.

3.4 Stress-strain curves

The second Piola-Kirchhoff (P-K) stresses were calculated within the frame of density functional theory at prescribed strains[36] and were plotted in Fig. 4 for uniaxial strains along the armchair and zigzag directions as well as the biaxial strains. The ultimate strength is defined as the maximum stress that a material can withstand while being stretched, which can be read from the stress-strain curves. The corresponding strain to the ultimate stress is the ultimate strain. The critical strain is larger than the ultimate strain under ideal conditions without defects and thermal vibrations. In other words, the systems of perfect silicane beyond ultimate strains are in a metastable state, which might be easily destroyed by factors including long wavelength perturbations, vacancy defects, and high temperature effects[60]. As a result, only the data within the ultimate strain has physical meaning, which we used in determining the high order elastic constants in the following subsection. The ultimate strains are still very important because they reflect the intrinsic bonding strengths. They are also useful since they act as a lower limit of the critical strain. Therefore they have practical meanings in consideration for the applications of silicane.

Table 2 Ultimate strengths Ultimate stresses (Σ_u^a,Σ_u^z,Σ_u^b), ultimate strains (η_u^a, η_u^z, η_u^b), and Young's modulus (Y^a,Y^z,Y^b) under uniaxial strain (armchair and zigzag) and biaxial of silicane from DFT calculations, compared with silicene and graphane.

	Silicane	Calc.[a]	Silicene[b]	graphane[c]
Y^a (N/m)	56.37	54.8		
Σ_u^a(N/m)	5.8	7.3	6.0	18.9
η_u^a	0.22	0.23	0.17	0.17
Y^z (N/m)	56.17	54.5		
Σ_u^z(N/m)	6.0	7.93	5.9	21.4
η_u^z	0.28	0.25	0.21	0.25
Y^b (N/m)	69.43			
Σ_u^b(N/m)	5.7		6.2	20.8
η_u^b	0.21		0.17	0.23

[a] Previous DFT study in Ref.[17]
[b] Low-buckling configuration in Ref.[5]
[c] Ref.[47]

Our results of the ultimate strengths and ultimate strains are summarized in Table 2, compared with those of silicene and graphane. All three materials behave in an asymmetric manner with respect to compressive and tensile strains. The compressive strains cause a more severe increase of stresses than tensile strains. Specifically, the stress applied on silicene is -10 N/m when a biaxial strain of -0.1 is applied (Fig. 4), whose magnitude is more than double of that at strain 0.1 (4.2 N/m), and about the twice of the ultimate strength of the material (5.7 N/m). We noticed that the large negative strains beyond -0.1 will cause unphysically large stresses. Consequently, we did not consider the compressive strains larger than 0.1 in this study.

Under tensile strains, the Si-Si bonds are stretched. With the increase of the bond lengths, the bonds are weakened, and eventually rupture. Such behaviors also have a direction dependent association with applied strains. When the strain is applied in the armchair direction, the bonds of those parallel in this direction are more severely stretched than those in other directions. The Si-H bonds are not affected since they are perpendicular to the strains. When the strain is applied along the zigzag direction, which is perpendicular to the armchair, there is no bond parallel to this direction, but instead inclined or perpendicular. The bonds at an incline to the zigzag direction are more severely stretched than those in the armchair direction. Under the ultimate strain, which is 0.28, the bonds at an

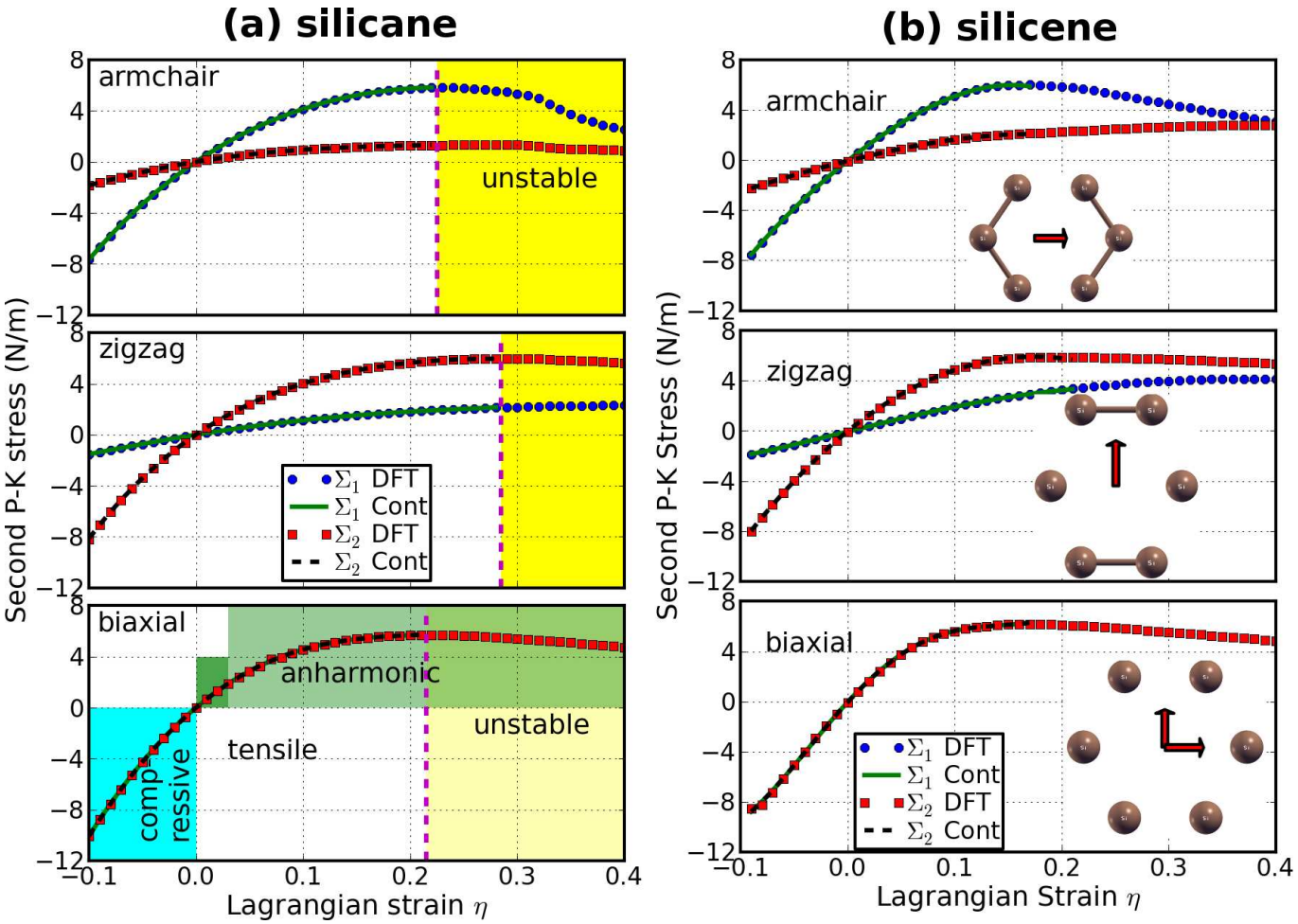

Fig. 4 Stress-strain responses. The stress-strain responses of **a** silicane monolayers compared to **b** silicene monolayers[5] under the *armchair* (top), *zigzag* (middle), and *biaxial* (bottom) strains. Σ_1 (Σ_2) denotes the x (y) component of stress. "Cont" stands for the fitting of DFT calculations ("DFT") to continuum elastic theory. The linear elastic and non-linear elastic regions are within the elastic limit defined by ultimate strains. The systems under strains beyond the elastic limits are unstable. The strain limits of silicane are 0.22, 0.28, and 0.21 for *armchair*, *zigzag*, and *biaxial* deformations, respectively, with the stress limits of 5.8, 6.0, and 5.7 N/m respectively.

incline to the armchair direction are observed to be ruptured (Fig. 4 middle). Under the ultimate strain in biaxial deformation which is η_m^b=0.21, all the Si-Si bonds are observed to be ruptured. This directional dependance of the ultimate strains reflect the chirality effects. Typically for a hexagonal lattice structure, zigzag direction tensile test can withstand more loading than armchair direction tensile test due to the chirality effects of both the bond angle variation and the bond length extension, which leads bond rotation in addition to elongation in the zigzag direction[61,62]. Our results of the chirality dependent mechanical properties agree well with the general trend as well as previous study in silicane nanoribbons[26].

Compared to silicene, the stress-strain responses show that all the ultimate tensile strengths (Σ_u^a,Σ_u^z,Σ_u^b) of silicane are very close to those of silicene, indicating that the hydrogenation from silicene to silicane has little effect on its ultimate tensile strengths. On the contrary, the ultimate strains increase by 29%, 33%, and 24% under armchair, zigzag, and biaxial deformations, respectively. Such an increase of the ultimate strains are due to the increase of the roughness of 59% of the hydrogenation.

It is worth noting that by applying the periodic boundary conditions for simulation boxes in size of nanometers, our model represents an infinite plane of silicane without any defect, which may not be materialized in practice. However, our results can serve as an upper limit of the nanoribbons of silicane in a real application.

3.5 Elastic Constants

The elastic constants play a central role in representing the mechanical properties of a material. In this study, the elastic constants, including high order elastic constants, were obtained from the stress-strain curves within the elastic regions (Fig. 4) by linkage between the elastic theory and the atomistic model. Based on the precise ab initio density functional theory calculations, our results of these elastic constants provide an accurate continuum description of the elastic properties of silicane, which are suitable for incorporation into numerical methods such as the finite element technique for macro scale modeling. We classified the elastic constants into second and higher order (> 2) elastic constants according to their linearity. The second order elastic constants model the linear elastic response while the higher order elastic constants are important to characterize the nonlinear elastic response. All the elastic constants up to 5th order are summarized in Table 3, compared with those values of silicene and graphane.

The in-plane stiffness Y_s is an important parameter in measuring a monolayer's strength. The Poisson ratio which is defined as the negative ratio of transverse to axial strain of the monolayer is also an important quantity for its mechanical properties. The in-plane stiffness and Poisson ratio ν

Table 3 Elastic constants Nonzero independent components for the second order elastic constants (SOECs), third order elastic constants (TOECs), fourth order elastic constants (FOECs), fifth order elastic constants (FFOECs), in-plane stiffness Y_s, and Poisson ratio ν of silicane from DFT calculations, compared with silicene and graphane.

	Silicane	Calc.[a]	Silicene[b]	Graphane[c]
Y_s	53.8	63.8	63.8	246.7
ν	0.240	0.240	0.325	0.078
C_{11}	57.1		71.3	248.2
C_{12}	13.7		23.2	19.4
C_{111}	-404.9		-397.6	-2374.1
C_{112}	-34.6		-14.1	-95.4
C_{222}	-349.6		-318.9	-2162.8
C_{1111}	2146		-830	19492
C_{1112}	-195		-309	819
C_{1122}	-107		-5091	68
C_{2222}	1240		-629	14823
C_{11111}	-7525		-20614	-103183
C_{11112}	2495		6923	816
C_{11122}	-1671		-11681	-16099
C_{12222}	-3318		-7593	-10151
C_{22222}	-4517		-29735	-134277

[a] Previous DFT calculations in Ref.[26]
[b] low-buckling configuration in Ref.[5]
[c] Ref.[47]

are closely related to the second order elastic constants as $Y_s = (C_{11}^2 - C_{12}^2)/C_{11}$ and $\nu = C_{12}/C_{11}$. For silicane, our results are $Y_s = 53.8$ (N/m) and $\nu = 0.240$, which are in good agreement with a previous *ab initio* study[26] as listed in Table 3. The in-plane stiffness of silicane is 84% of that of silicene, which indicates that the silicene is softened by the hydrogenation to silicane. This could be understood as follows. The Si-Si bond length in silicane is 2.36 Å, about 3.5% larger than that of silicene (2.28 Å), which implies that the Si-Si bonds in silicene have been stretched by the introduction of hydrogen atoms *in priori*. These stretched Si-Si bonds are weaker than those un-stretched, resulting a reduction of the mechanical strength.

Besides the in-plane stiffness, the hydrogenation also reduces the Poisson ratio, by a factor of 26% from silicene to silicane. As shown in Fig. 1, the Si-H bonds are perpendicular to the plane. These stiff "arms" (Si-H bonds) result in a low Poisson ratio through in-plane bending modes, involving the Si-Si-Si angles. In principle, it could cause a strong anharmonic coupling of the out-of plane bending mode with these in-plane bending accordion modes, which reduces the out-of-plane strains as the in-plane strains are applied. A recent review paper also reports that materials with stiff arms or struts in directions normal to the loading axis will resist transverse contraction and exhibit low Poisson ratios[63]. The reduction of both mechanical strengths and the Poisson ratio is also observed in the hydrogenation of graphene to graphane[47].

Our results show that silicane monolayers are mechanically stable under tensile strains of 0.21. The mechanical instability shows up at larger tension. Their stress-strain curves show that they will soften when the strain is larger than the ultimate strain. The increased strains reduce the stresses due to bonds weakening and breaking at the atomic level. In the continuum aspect, this softening behavior is determined by the third and fifth-order elastic constants. The negative values of the third-order elastic constants and the fifth-order elastic constants ensure the softening of the silicane monolayer under large strain.

Using the higher order elastic continuum description, one can calculate the stress and deformation state under uniaxial stress, rather than uniaxial strain. Explicitly, when pressure is applied, the pressure dependent second-order elastic moduli can be obtained from the higher order elastic continuum description[36]. The third-order elastic constants are important in understanding the nonlinear elasticity of materials, such as changes in acoustic velocities due to finite strain. As a consequence, nano devices (such as nano surface acoustic wave sensors and nano waveguides) could be synthesized by introducing local strain[64,65].

A good way to check the importance of the high order elastic constants is to consider the cases when they are missing. With the elastic constants, the stress-strain response can be predicted from elastic theory[36]. When we only consider the second order elasticity, the stress varies with strain linearly. Take the biaxial deformation as an example. As illustrated in Fig. 5, the linear behaviors are only valid within a small strain range, about $\eta_h = 0.02$, the same result obtained from the energy versus strain curves in Fig. 3. With the knowledge of the elastic constants up to the third order, the stress-strain curve can be accurately predicted within the range of $\eta \leq 0.08$. Using the elastic constants up to the fourth order, the mechanical behaviors can be well treated up to a strain as large as 0.13. For the strains beyond 0.13, the fifth order elastic are required for accurate modeling. The analysis of the uniaxial deformations provides similar results.

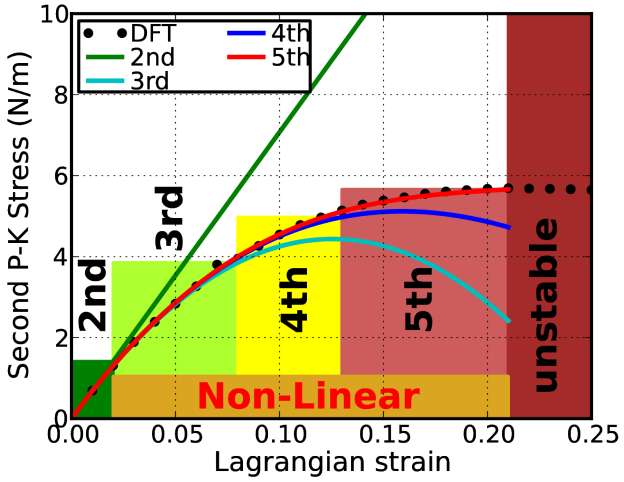

Fig. 5 Limits of higher order effects. Predicted stress-strain responses of *biaxial* deformation of silicane from different orders of elastic constants. comparing with density functional theory (DFT) calculations (dotted line) indicates the limitations are 0.02, 0.08, 0.13, and 0.21 for second, third, fourth, and fifth order elastics, respectively.

Furthermore, our result also illustrated that the non-linear elastic behavior is prominent in the two-dimensional nanomaterials compared to the linear elastic behavior (Fig. 5). This is very different from their macro-scale counterparts, where non-linear elastic region is only within the strain of 0.01 beyond the linear elastic region. Such prominent non-linear elastic behaviors are commonly spotted in other nanostructures. The underlying reason could be that there are much less defects inside the nanostructures than the bulk materials. For the same reason, a similar non-linear behavior of perfect bulk aluminum was observed in a DFT study for hydrostatic type strains[66].

It is worthy to mention that our results of mechanical properties of silicane are restricted to zero temperature. At finite temperatures, the thermal expansions and dynamics will in general reduce the interactions between atoms. One can expect that the longitudinal mode elastic constants will decrease with respect to the temperature of the system. However, the

variation of shear mode elastic constants might be more complex in response to temperature, which deserve further studies.

3.6 Pressure effect on the elastic moduli

Same as strains, pressure engineering is also a "clean" approach to tailor the functions and properties by mechanical load without introducing alien species[25]. Thus it is also important to know the pressure effect on the elastic moduli, which could be achieved through elastic theory with the knowledge of the higher order elastic constants. With third-order elastic moduli, As demonstrated in the following, the effect of pressure p on the second-order elastic moduli of the silicane monolayers can be obtained with third-order elastic moduli. It is worth noting that the pressure p acts in the plane of silicane. When pressure is applied, the pressure dependent second-order elastic moduli ($\tilde{C_{11}}$, $\tilde{C_{12}}$, $\tilde{C_{22}}$) can be obtained from C_{11}, C_{12}, C_{22}, C_{111}, C_{112}, C_{222}, Y_s, and ν[64,65].

Our results of the pressure effect on the second-order elastic moduli are illustrated in Fig. 6 for the silicane monolayers. There is a general trend that these second-order elastic moduli increase linearly with the applied pressure. However, Poisson's ratio decreases monotonically with the increase of pressure, which means that silicane monolayers are more easily compressed than sheared under a higher pressure. In addition, $\tilde{C_{11}}$ is not symmetrical to $\tilde{C_{22}}$ any more under pressure. Only when $P = 0$, $\tilde{C_{11}} = \tilde{C_{22}} = C_{11}$. This anisotropy could be the outcome of anharmonicity. We notice that the pressure effects on the elastic moduli of silicane have similar trends as that on silicene, however with a smaller magnitude. Furthermore, the hydrogenation does not change the monotonic decrement of the Poisson ratio with increasing pressure. Our results illustrate that the hydrogenation affects the elastic behaviors of silicene under pressure.

To the authors' best knowledge, the synthesis of silicane has not been reported. The successful synthesis of silicane depends on many factors. Our computational study shows that silicane is mechanically stable in ideal cases without any defects, which is invaluable to experiments since it points out that silicane could be synthesized when defects are well treated. In addition, our results of the elastic limits of silicane monolayers also provide a safe guide for their promising applications, as well as strain engineering their functions and properties.

The electron mobility in silicane is predicted to scale with the inverse average effective mass at the conduction band minimum[27]. The increasing uniaxial strain along the armchair direction and biaxial strain keep increasing the electron mobility. Counting in the large ultimate strains, silicane is a promising high-mobility semiconductor under strain engineering, such as High-electron-mobility field-effect transistor, for next-generation electronics.

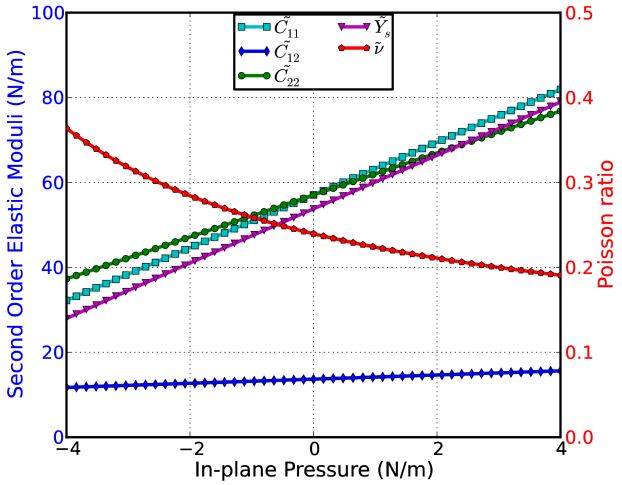

Fig. 6 Pressure effect Second-order elastic constants, in-plane stiffness, and Poisson ratio as a function of the pressure in the plane of silicane monolayers.

4 CONCLUSIONS

We studied the elastic limits of silicane under various strains using first-principles calculations based on density functional theory. It was observed that silicane exhibits a nonlinear elastic deformation up to an ultimate strain, which is 0.22, 0.28, and 0.25 for armchair, zigzag, and biaxial directions, respectively. Silicane was observed to have a relatively low in-plane stiffness (53.8 N/m) and a low Poisson ratio (0.24) compared to silicene, which indicates that the full hydrogenation of the silicene reduced its intrinsic strength by a factor of 16% and its Poisson ratio by 26%. However, such hydrogenation has little effect on its ultimate tensile strengths. On the contrary, the ultimate strains increase by 29%, 33%, and 24% under armchair, zigzag, and biaxial deformations, respectively. Such increase in the ultimate strains are due to the increase of the buckling roughness of 59% of the hydrogenation.

We also investigated the nonlinear mechanical properties and the mechanical instabilities of silicane. By linking the elastic theory with precise first-principles calculations, we obtained an accurate continuum description of the elastic properties which is suitable for a finite element analysis model for its applications at large scale. The fourteen independent components of high order (up to fifth order) elastic constants are determined from the fitting of the stress-strain curves from DFT calculations. We also found that the harmonic elastic constants are only valid with a small range of -0.02 $\leq \eta \leq$ 0.02. With the knowledge of the elastic constants up to the third order, the stress-strain curve can be accurately predicted within the range of $\eta \leq 0.08$. Using the elastic constants up to the fourth order, the mechanical behaviors can be accurately predicted

up to a strain as large as 0.13. For the strains beyond 0.13, the fifth order elastic constants are required for accurate modeling. The second-order elastic constants linearly increase with applied in-plane pressure and the Poisson's ratio monotonically decreases with increasing pressure. The pressure effect on the second-order elastic constants and the in-plane stiffness of silicane are less than those of silicene.

ACKNOWLEDGEMENTS

The authors would like to acknowledge the generous financial support from the Defense Threat Reduction Agency (DTRA) Grant # BRBAA08-C-2-0130 and # HDTRA1-13-1-0025.

Author Contribution Statement

Q.P. and S.D. designated the research topic. Q. P. conducted the calculations and wrote the main manuscript text. All authors reviewed the manuscript.

Competing Financial Interests

The authors declare no competing financial interests.

References

1 P. De Padova, C. Quaresima and et. al., *Appl. Phys. Lett.*, 2010, **96**, 261905.

2 A. Kara, H. Enriquez, A. P. Seitsonen, L. C. L. Y. Voon, S. Vizzini, B. Aufray and H. Oughaddou, *Surf. Sci. Rep.*, 2012, **67**, 1–18.

3 P. Vogt, P. De Padova, C. Quaresima, J. Avila, E. Frantzeskakis, M. C. Asensio, A. Resta, B. Ealet and G. Le Lay, *Phys. Rev. Lett.*, 2012, **108**, 155501.

4 T. Morishita, K. Nishio and M. Mikami, *Phys. Rev. B*, 2008, **77**, 081401.

5 Q. Peng, J. Crean, A. K. Dearden, X. Wen, C. Huang, S. P. A. Bordas and S. De, *Mod. Phys. Lett. B*, 2013, **27**, 1330017.

6 Q. Peng, X. Wen and S. De, *RSC Adv.*, 2013, **3**, 13772 – 13781.

7 M. Xu, T. Liang, M. Shi and H. Chen, *Chem. Rev.*, 2013, **113**, 3766–3798.

8 D. Jose and A. Datta, *Acc. Chem. Res.*, 2013, **0**, null.

9 J. Gao, J. Zhang, H. Liu, Q. Zhang and J. Zhao, *Nanoscale*, 2013, **5**, 9785–9792.

10 T. Hussain, T. Kaewmaraya, S. Chakraborty and R. Ahuja, *Phys. Chem. Chem. Phys.*, 2013, **15**, 18900–18905.

11 F. Li, C.-w. Zhang, H.-x. Luan and P.-j. Wang, *J. Nanopart. Res.*, 2013, **15**, 1972.

12 J. Wang, J. Li, S.-S. Li and Y. Liu, *J. Appl. Phys.*, 2013, **114**, year.

13 O. Pulci, P. Gori, M. Marsili, V. Garbuio, R. Del Sole and F. Bechstedt, *Euro. Phys. Lett.*, 2012, **98**, year.

14 D. Kaltsas, T. Tsatsoulis, O. G. Ziogos and L. Tsetseris, *J. Chem. Phys.*, 2013, **139**, year.

15 W. Wei and T. Jacob, *Phys. Rev. B*, 2013, **88**, 045203.

16 W. Wei, Y. Dai, B. Huang and T. Jacob, *Phys. Chem. Chem. Phys.*, 2013, **15**, 8789–8794.

17 C. Gang, L. Peng-Fei and L. Zi-Tao, *Chin. Phys. B*, 2013, **22**, year.

18 J. Kim, M. V. Fischetti and S. Aboud, *Phys. Rev. B*, 2012, **86**, 205323.

19 L. Pan, H. J. Liu, Y. W. Wen, X. J. Tan, H. Y. Lv, J. Shi and X. F. Tang, *Appl. Surf. Sci.*, 2012, **258**, 10135–10139.

20 L. C. L. Y. Voon, E. Sandberg, R. S. Aga and A. A. Farajian, *Appl. Phys. Lett.*, 2010, **97**, 163114.

21 M. Houssa, E. Scalise, K. Sankaran, G. Pourtois, V. V. Afanas'ev and A. Stesmans, *Appl. Phys. Lett.*, 2011, **98**, year.

22 J. C. Garcia, D. B. de Lima, L. V. C. Assali and J. F. Justo, *J. Phys. Chem. C*, 2011, **115**, 13242–13246.

23 Y. Ding and Y. Wang, *Appl. Phys. Lett.*, 2012, **100**, –.

24 C.-w. Zhang and S.-s. Yan, *J. Phys. Chem. C*, 2012, **116**, 4163–4166.

25 F. Guinea, M. I. Katsnelson and A. K. Geim, *Nat. Phys.*, 2010, **6**, 30–33.

26 H. Zhao, *Phys. Lett. A*, 2012, **376**, 3546–3550.

27 O. D. Restrepo, R. Mishra, J. E. Goldberger and W. Windl, *J. Appl. Phys.*, 2014, **115**, 033711.

28 Y. Hiki, *Annual Review of materials science*, 1981, **11**, 51.

29 K. Brugger, *J. Appl. Phys.*, 1965, **36**, 768.

30 Q. Peng and S. De, *Phys. Chem. Chem. Phys.*, 2013, **15**, 19427 – 19437.

31 C. Lee, X. Wei, J. W. Kysar and J. Hone, *Science*, 2008, **321**, 385–388.

32 C. A. Marianetti and H. G. Yevick, *Phys. Rev. Lett.*, 2010, **105**, 245502.

33 G. Kresse and J. Hafner, *Phys. Rev. B*, 1993, **47**, 558.

34 J. Perdew, K. Burke and M. Ernzerhof, *Phys. Rev. Lett.*, 1996, **77**, 3865.

35 P. E. Blöchl, *Phys. Rev. B*, 1994, **50**, 17953–17979.

36 Q. Peng, W. Ji and S. De, *Comput. Mater. Sci.*, 2012, **56**, 11 – 17.

37 X. Wei, B. Fragneaud, C. A. Marianetti and J. W. Kysar, *Phys. Rev. B*, 2009, **80**, 205407.

38 Q. Peng, X.-J. Chen, S. Liu and S. De, *RSC Adv.*, 2013, **3**, 7083–7092.

39 Q. Peng, C. Liang, W. Ji and S. De, *Mech. Mater.*, 2013, **64**, 135–141.

40 Q. Peng, X.-J. Chen, W. Ji and S. De, *Adv. Eng. Mater.*, 2013, **15**, 718–727.

41 Q. Peng, C. Liang, W. Ji and S. De, *Appl. Phys. A*, 2013, **13**, 483–490.

42 Q. Peng, C. Liang, W. Ji and S. De, *Comput. Mater. Sci.*, 2013, **68**, 320–324.

43 Q. Peng and S. De, *RSC Adv.*, 2013, **3**, 24337 – 24344.

44 H. Nakano, O. Ohtani, T. Mitsuoka, Y. Akimoto and H. Nakamura, *J. Am. Ceram. Soc.*, 2005, **88**, 3522–3524.

45 U. Dettlaff-Weglikowska, W. Hönle, A. Molassioti-Dohms, S. Finkbeiner and J. Weber, *Phys. Rev. B*, 1997, **56**, 13132–13140.

46 J. R. Dahn, B. M. Way, E. Fuller and J. S. Tse, *Phys. Rev. B*, 1993, **48**, 17872–17877.

47 Q. Peng, C. Liang, W. Ji and S. De, *Phys. Chem. Chem. Phys.*, 2013, **15**, 2003–2011.

48 B. Cordero, V. Gomez, A. E. Platero-Prats, M. Reves, J. Echeverria, E. Cremades, F. Barragan and S. Alvarez, *Dalton Trans.*, 2008, 2832–2838.

49 S. Cahangirov, M. Topsakal, E. Akturk, H. Sahin and S. Ciraci, *Phys. Rev. Lett.*, 2009, **102**, 236804.

50 P. Giannozzi, S. Baroni, N. Bonini, M. Calandra, R. Car, C. Cavazzoni, D. Ceresoli, G. L. Chiarotti, M. Cococcioni, I. Dabo, A. Dal Corso, S. de Gironcoli, S. Fabris, G. Fratesi, R. Gebauer, U. Gerstmann, C. Gougoussis, A. Kokalj, M. Lazzeri, L. Martin-Samos, N. Marzari, F. Mauri, R. Mazzarello, S. Paolini, A. Pasquarello, L. Paulatto, C. Sbraccia, S. Scandolo, G. Sclauzero, A. P. Seitsonen, A. Smogunov, P. Umari and R. M. Wentzcovitch, *J. Phys.:Condens. Matter.*, 2009, **21**, 395502 (19pp).

51 E. Scalise, M. Houssa, G. Pourtois, B. van den Broek, V. Afanasev and A. Stesmans, *Nano Research*, 2013, **6**, 19–28.

52 Y. Ding and Y. Wang, *Appl. Phys. Lett.*, 2012, **100**, 083102.

53 E. Cerda and L. Mahadevan, *Phys. Rev. Lett.*, 2003, **90**, 074302.

54 Y. Zhang and F. Liu, *Appl. Phys. Lett.*, 2011, **99**, 241908.

55 G. Tsoukleri, J. Parthenios, K. Papagelis, R. Jalil, A. C. Ferrari, A. K. Geim, K. S. Novoselov and C. Galiotis, *Small*, 2009, **5**, 2397–2402.

56 W. Bao, F. Miao, Z. Chen, H. Zhang, W. Jang, C. Dames and C. N. Lau, *Nat. Nanotech.*, 2009, **4**, 562–566.

57 D. Yoon, Y.-W. Son and H. Cheong, *Nano Lett.*, 2011, **11**, 3227–3231.

58 W. Pan, J. Xiao, J. Zhu, C. Yu, G. Zhang, Z. Ni, K. Watanabe, T. Taniguchi, Y. Shi and X. Wang, *Sci. Reports*, 2012, **2**, 893.

59 R. Quhe, J. Zheng, G. Luo, Q. Liu, R. Qin, J. Zhou, D. Yu, S. Nagase, W.-N. Mei, Z. Gao and J. Lu, *NPG Asia Mater.*, 2012, **4**, E6.

60 M. Topsakal, S. Cahangirov and S. Ciraci, *Appl. Phys. Lett.*, 2010, **96**, 091912.

61 F. Liu, P. Ming and J. Li, *Phys. Rev. B*, 2007, **76**, 064120.

62 H. Zhao, K. Min and N. R. Aluru, *Nano Lett.*, 2009, **9**, 3012–3015.

63 G. N. Greaves, A. L. Greer, R. S. Lakes and T. Rouxel, *Nat. Mater.*, 2011, **10**, 823–837.

64 Q. Peng, A. R. Zamiri, W. Ji and S. De, *Acta Mechanica*, 2012, **223**, 2591–2596.

65 Q. Peng, W. Ji and S. De, *Phys. Chem. Chem. Phys.*, 2012, **14**, 13385–13391.

66 M. Iyer, V. Gavini and T. M. Pollock, *Phys. Rev. B*, 2014, **89**, 014108.